Optics and Lasers in Engineering 152 (2022) 106953

Contents lists available at ScienceDirect

Optics and Lasers in Engineering

journal homepage: www.elsevier.com/locate/optlaseng

Measurement sensitivity of DUV scatterfield microscopy parameterized with partial coherence for duty ratio-varied periodic nanofeatures

Eikhyun Cho[a,1], Taekyung Kim[a,1], Yoon Sung Bae[a], Sang-Soo Choi[b], Bryan M. Barnes[a], Richard M. Silver[a], Martin Y. Sohn[a,*]

[a] Physical Measurement Laboratory, National Institute of Standards and Technology, 100 Bureau Drive, Gaithersburg, MD 20899, USA
[b] PKL-Photronics, 493-3 Sungsung-Dong, Seobukgu, Cheonan, Choongnam, South Korea

ARTICLE INFO

Keywords:
Scatterfield microscopy
Measurement sensitivity
Critical dimension
Partial coherence
Duty ratio

ABSTRACT

The deep ultraviolet (DUV) scatterfield imaging microscopy technique enables accurate dimensional measurements of periodic nanostructures with sub-nanometer sensitivity to support semiconductor device manufacturing. A parametric sensitivity analysis for targets with uneven duty ratios is essential as the duty ratios of many periodic nanostructures vary in practice. This paper presents an experimental implementation to optimize illumination conditions for nanoscale multi-line targets on a Molybdenum Silicide (MoSi) photomask with duty ratios of 0.43 to 0.68 using a scatterfield imaging microscope with 193 nm wavelength laser designed for angle-resolved illumination at the sample. Measurement sensitivities are analyzed using sensitivity coefficient maps parameterized by partial coherence factor, duty ratio of the target, and incident polarization.

1. Introduction

High-sensitivity dimensional measurement tools for critical dimensions (CDs) and defects are critical to the quality control of the fabrication process of nanoscale devices such as integrated circuits, display devices, and metasurfaces [1–3]. Optical scatterfield imaging microscopy, which incorporates scatterometry into traditional optical imaging microscopy, has been demonstrated as a novel technique for nanofeature characterization with high sensitivity even for deep subwavelength features well beyond the conventional resolution limit [4–9]. This technique retains multiple benefits of traditional optical microscopy such as high measurement throughput, non-destructive measurement, and low operational cost relative to nanoscale scanning probe measurement techniques such as scanning electron microscopy (SEM), atomic force microscopy (AFM), scanning tunneling microscopy (STM), and scanning near-field optical microscopy (SNOM) [10–13]. Using this technique, nanoscale dimensional characterization has been achieved with high sensitivity by analyzing the scattered far-field images and least squares regression using model libraries [7,9,14,15].

In scatterfield imaging microscopy, the coherence in the spatial domain is an adjustable parameter that has a great influence on the imaging performance. Thus, it is essential to characterize and understand how spatial coherence affects optical system performance. The degree of partial coherence is a crucial factor in other emerging phase imaging techniques such as quantitative phase imaging (QPI) [16] as well as ptychography [17].

We have previously reported the effects of partial coherence on dimensional measurement sensitivity using a deep ultraviolet (DUV) scatterfield microscope platform to address illumination optimization for high sensitivity [18]. Although the partial coherence was demonstrated to be an important parameter for enhancing measurement sensitivity, the experiments were limited to targets with a fixed ratio between linewidths and their periodicity, also referred to as duty cycle or duty ratio. Including duty ratio variation is essential as many nanoscale device features including integrated circuits, display devices, and metasurfaces possess unequal duty ratios [19–24].

In this paper, we present an empirical study of dimensional measurement sensitivity for partial coherence variation with respect to CDs on a Molybdenum Silicide (MoSi) photomask in which the structures consist of linewidths having uneven duty ratios. Sensitivities were measured and analyzed with two different polarizations and six different partial coherence factors. Based on the measured values, partial coherence factors have been optimized to yield the highest CD measurement sensitivity. This study suggests a methodology to improve the measurement sensitivity of DUV scatterfield microscopy by optimizing the illumination without the regression process of experimental data using a simulated data set, thus complementing the full scatterfield imaging microscopy measurements.

* Corresponding author.
E-mail address: martin.sohn@nist.gov (M.Y. Sohn).
[1] These authors contributed equally to this work.

https://doi.org/10.1016/j.optlaseng.2022.106953
Received 6 August 2021; Received in revised form 7 January 2022; Accepted 10 January 2022

2. Measurement sensitivity of scatterfield microscopy

Optical scatterfield microscopy relies on scattered light resulting from sophisticated illumination based on a Köhler geometry that correlates the spatial position at the conjugate back focal plane (CBFP) of the objective lens (OL) to the incident ray angle at the target plane, enabling the control of illumination shape or angle, as shown in Fig. 1(a) [25–27]. An illumination light ray originating at a position at the CBFP is directed to the sample plane (SP) with a corresponding angle, enabling resolved illumination tailored to a sample and the reflected scattered light. Satterfield images taken at the charge coupled device (CCD), which result from various illumination conditions such as angle-resolved illumination, focus variation, phase shifting, or polarization, yields the structure information of nanoscale targets through parametric comparison using model-based electromagnetic simulations. Dimensional measurement sensitivity of the nanoscale targets beyond the diffraction limit can be evaluated through comparing two intensity profiles obtained at the CCD for two periodic targets with different dimensions. The sensitivity changes as the illumination scheme are varied for different partial coherence factors, σ, which are defined as the ratio of illumination to collection numerical aperture (NA), and corresponds to the illumination coherence degree with a low partial coherence factor implying higher coherence and vice versa [9,28–33].

Fig. 1(b) shows the conceptual schematic of the dimensional measurement sensitivity changes with respect to nanoscale periodic lines having different duty ratios and partial coherence factors. The finite multiple line target group A and B have different pitch values P_A and P_B with a same set of linewidth values L_{1-3}. Intensity profiles have central valleys or hills for the line scattering and spikes for the boundary between lines and substrate [9,16]. Each set of intensity profiles for the group A and B show height differences due to the change of linewidth L, which are used to evaluate the measurement sensitivities. The sensitivity is evaluated in terms of the sensitivity coefficient, which is described as

$$c = \frac{\partial I}{\partial L} \tag{1}$$

where, I and L are the intensity height and the dimension measurand of the target, respectively [34–37]. The magnitude of I is the difference between the averaged intensity of the multiline region and the averaged intensity from the substrate. The bigger the height difference between intensity profiles for differing linewidths at a fixed pitch, the better sensitivity the measurement achieves. Illumination with a lower partial coherence factor induces the obvious spikes at the multiline area border due to the higher coherence, while a higher partial coherence factor yields a smoother profile due to the lower coherence. However, the intensities at the target edge region are excluded here from the quantitative sensitivity coefficient evaluation, as there is a discrepancy in intensities between the edge and the multiline regions. The intensity at the multiline region is governed mainly by the partial coherence and line structure, while the intensity at the edge is governed by not only the partial coherence but also the complex boundary condition between the substrate and finite multiline regions [33].

3. Experimentation

The experimental setup for DUV scatterfield imaging microscopy consists of illumination, collection, and navigation optics as shown in Fig. 2(a), and the experiments were conducted in a class 10 cleanroom to prevent the nanoscale samples from contamination. An ArF Excimer laser of a wavelength of 193.3 nm is used as the light source, which requires the optics and beam paths to be enclosed and purged with dry nitrogen gas to reduce ozone formation and to minimize contamination for maintaining the required optical performance. Although DUV incurs higher operational costs and require a specialized environment for the DUV-based optical system, there are unique benefits of using DUV source. First, the objective lens with DUV light collects more scattered orders from the nanoscale features than from visible light, enabling better analysis of various geometrical parameters and thus high sensitivity and low uncertainty can be achieved. Second, here the shorter wavelength sources enable the scatterfield imaging microscope to capture clearer scatterfield-based image of the whole target shape which has dimensions smaller than the resolution limit at visible wavelengths. Finally, in addition to the CD metrology, the DUV scatterfield imaging microscopy has enabled sub-20 nm width measurements of patterning defects, beyond the capabilities of visible scatterfield imaging microscopes. The system specifications are summarized in Table 1.

The illumination optics are designed to be telecentric for both CBFP and sample plane (SP) based on Köhler illumination, allowing planar access to the CBFP for parallel scanning of a circular aperture or placing more complex non-circular apertures corresponding to resolved illumination. The telecentric CBFP is designed to have a relatively large diameter of 11.6 mm to enhance detailed control of the illumination shape [38]. The effective source (ES) is formed by the Beam Shaper Optics, which consists of a pair of cylindrical lenses, a circular aperture (CA), and a rotating diffuser (RD), and transfers the rectangular beam of 1 mm × 3 mm emitted from the 193 nm Excimer Laser to a diverging extended circular beam with 2 mm diameter and 0.12 NA. The RD, which rotates at a speed optimized for low-speckle illumination, is placed on a local isolation plate to avoid transferring rotation-induced vibration to the target and optical components [39,40]. Rectangular apertures mounted in a motorized rotating wheel are located at the CBFP to manipulate the illumination NA and shape at the sample plane, tailoring scatterfield light by selecting an aperture with a size corresponding to a specific partial coherence factor. The apertures have horizontal widths (x-axis) of 2 mm, 4 mm, 6 mm, 8 mm, 10 mm and 11.6 mm with a fixed vertical (y-axis) width of 11.6 mm. Fig. 2(b) shows the aperture shapes and the quantitative relation of the aperture width to the partial coherence factor and corresponding illumination angles with respect to the objective lens OL_S, which has an 8 mm working distance and a catadioptric structure with NA 0.13–0.74. The illumination polarization direction is aligned by the polarizer (P) along x or y axis relative to the line direction as shown in Fig. 3(b).

The collection optics collects scattered light field at the target through OL_S and transfers them to DUV CCD with a magnification of about 350 by the tube lens (TL), yielding a field of view (FOV) of 19.2 μm × 25.6 μm. The DUV CCD pixels with 14 μm pitch to form scatterfield image correspond to 40 nm at the sample plane.

The navigation optics supplements the collection optics by allowing a search function and access to the desired targets due to the inability of the collection optics to change magnification as the non-standard OL_S cannot be positioned repeatably using a rotating turret. A light emitting device (LED) of 463 nm wavelength as a source illuminates the sample through a visible objective OL_N and collects the sample images at the visible charge coupled device (VCCD) of 3.45 μm pixel resolution with a magnification of 10 and FOV of 845 μm × 707 μm. Once the desired target image is taken at the navigation optics center, the stage with 150 mm travel and 1 nm resolution moves the target to the collection optics center according to the calibrated coordinate difference between OL_S and OL_N.

The scatterfield image measurements are performed for a MoSi photomask fabricated by e-beam lithography as shown in Fig. 3. The targets are separated by a 200 μm period and distributed in column and row by pitch and linewidth variations of 10 nm and 4 nm, respectively, as shown in Fig. 3(a). Each target consists of 30 lines and are aligned along the vertical (y-axis) direction of the rectangular aperture as shown in Fig. 3(b). The measurement sensitivity coefficients are measured for the target pairs of 60 nm, 64 nm and 64 nm, 68 nm linewidths, which correspond to the intensity differences $|I_{64}- I_{60}|$ and $|I_{68}- I_{64}|$ in the scatterfield images. We obtained the difference between the averaged intensity of the multiline region and the averaged intensity of the bottom substrate without considering ringing artifacts in the edge of the patterns for quantitative sensitivity coefficient evaluation. In general the small change in

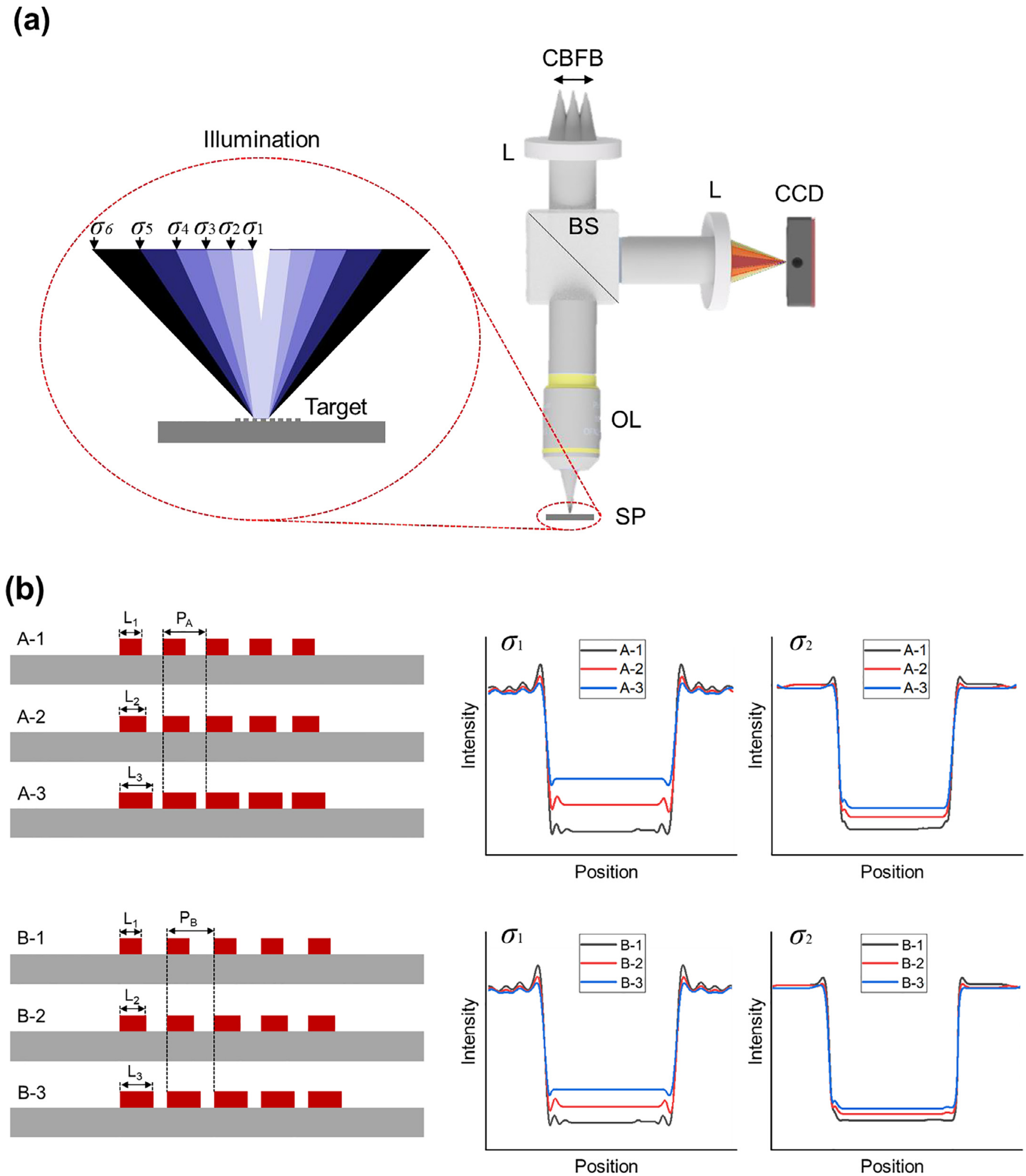

Fig. 1. Scatterfield microscopy metrology parameterized with partial coherence factor. (a) Scatterfield microscopy; CBFP – conjugate back focal plane, BS - beam splitter, OL - objective lens, SP - sample plane, L – lens. (b) Sensitivity for nanoscale periodic lines with varied duty ratios (linewidth L divided by pitch P). The variations of duty ratio L/P and partial coherence factor σ deviate the intensity height differences induced by the linewidth variation.

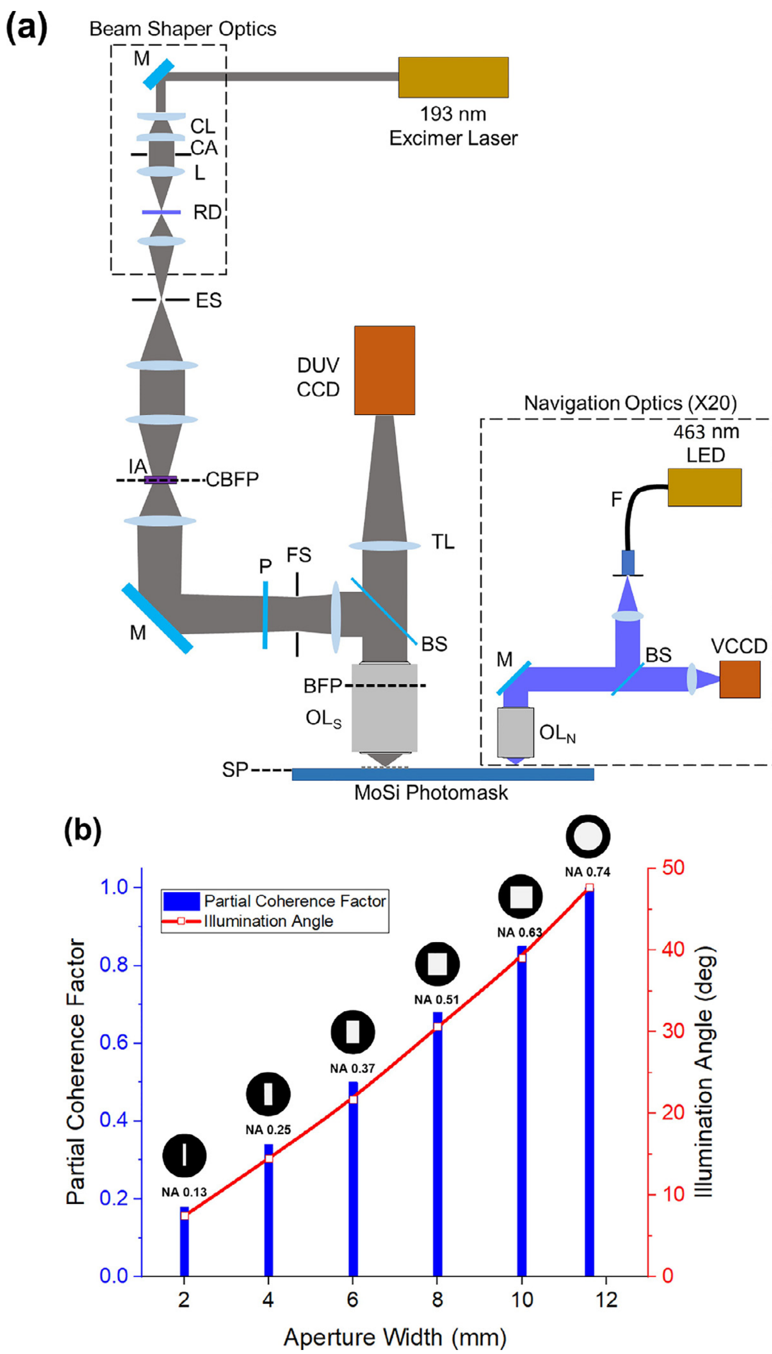

Fig. 2. DUV scatterfield imaging microscopy. (a) Schematic of experimental setup; M - mirror, CL - cylindrical lens pair, CA - circular aperture, L - lens, RD - rotating diffuser, ES - effective source, IA – illumination aperture, CBFP - conjugate back focal plane, P - polarizer, FS - field stop, BS - beam splitter, TL - tube lens, BFP – back focal plane, OLs - objective lens for scatterfield, SP - sample plane, OL_N - objective lens for navigation, F - fiber, VCCD - visible CCD. (b) Relationship of CBFP aperture width to the partial coherence factor and corresponding maximum illumination angle.

linewidth, ∂L can be set to 1% of measurand [35], which here would be 0.60 nm. However, the target fabrication for this change is difficult to achieve with e-beam lithography as used in the presented study. To this end, targets were printed with a linewidth differentiation of 4 nm, or about 6% of the measurands in a linewidth region for which the optical response appears monotonic with linewidth.

4. Results and discussion

Scatterfield intensity profiles for duty ratio-varied multiline targets with 3 linewidths and 5 pitches were measured to investigate the relationship of measurement sensitivity to partial coherence factor, as shown in Fig. 4. The two sets of 5 × 6 graph matrices for x and y polarized illuminations, which correspond to directions perpendicular and parallel to the target lines, show scattered intensity shapes of valley and hill at the line areas due to the scattering effect combined with Fresnel reflection. Columns and rows of the matrices represent varied pitches and partial coherence factors, respectively. Each intensity profile is obtained by normalization process with respect to the intensity average at the substrate area. As a first step, we obtained the average pixel value of the substrate (pixel averaging on the left and right sides of the patterned area). Then, we divided each pixel intensity value by average substrate intensity to obtain a normalized intensity. The normalized intensity can be calculated by Eq. (2),

$$I_{norm} = \frac{I_m}{\frac{\sum_{i=1}^{n} I_{sub(i)}}{n}} \tag{2}$$

where, I_{norm}, I_m, I_{sub}, n are normalized intensity, measured intensity, the measured intensity of the substrate, and a number of pixels in a line profile from the substrate, respectively. Each graph compares three

Table 1
Major specifications of 193 nm scatterfield microscope.

Parts	Items	Values
Illumination	193 nm Excimer laser	λ = 193.3 nm, spectral width 0.3 nm, 10 ns pulse
	Beam quality shaping	Cylindrical lens pair & rotating diffuser
	Effective source	2 mm dia.
	Telecentric CBFP	11.6 mm dia.
	Field of view (FOV)	Typical 50 μm dia., Maximum 120 μm dia.
	NA (Catadioptric OL)	0.13 - 0.74
	Working distance	≈ 8 mm
Collection	CCD	640 × 480 pixels w/ 14 μm period, QE ≈ 60% @193 nm
	Magnification	× 350
	Effective pixel size	40 nm
	Field of View	19.2 × 25.6 μm^2
Navigation	LED Source	λ = 463 nm
	Objective Lens	Working Distance = 28 mm
	Magnification	×10
	Field of view (FOV)	845 × 707 μm^2
Stages	Transverse (x, y)	150 mm travel, 1 nm resolution
	Rotational (θ)	0.1 m° resolution
	Vertical (coarse 3z, fine 3z)	25 mm travel, 1 nm resolution

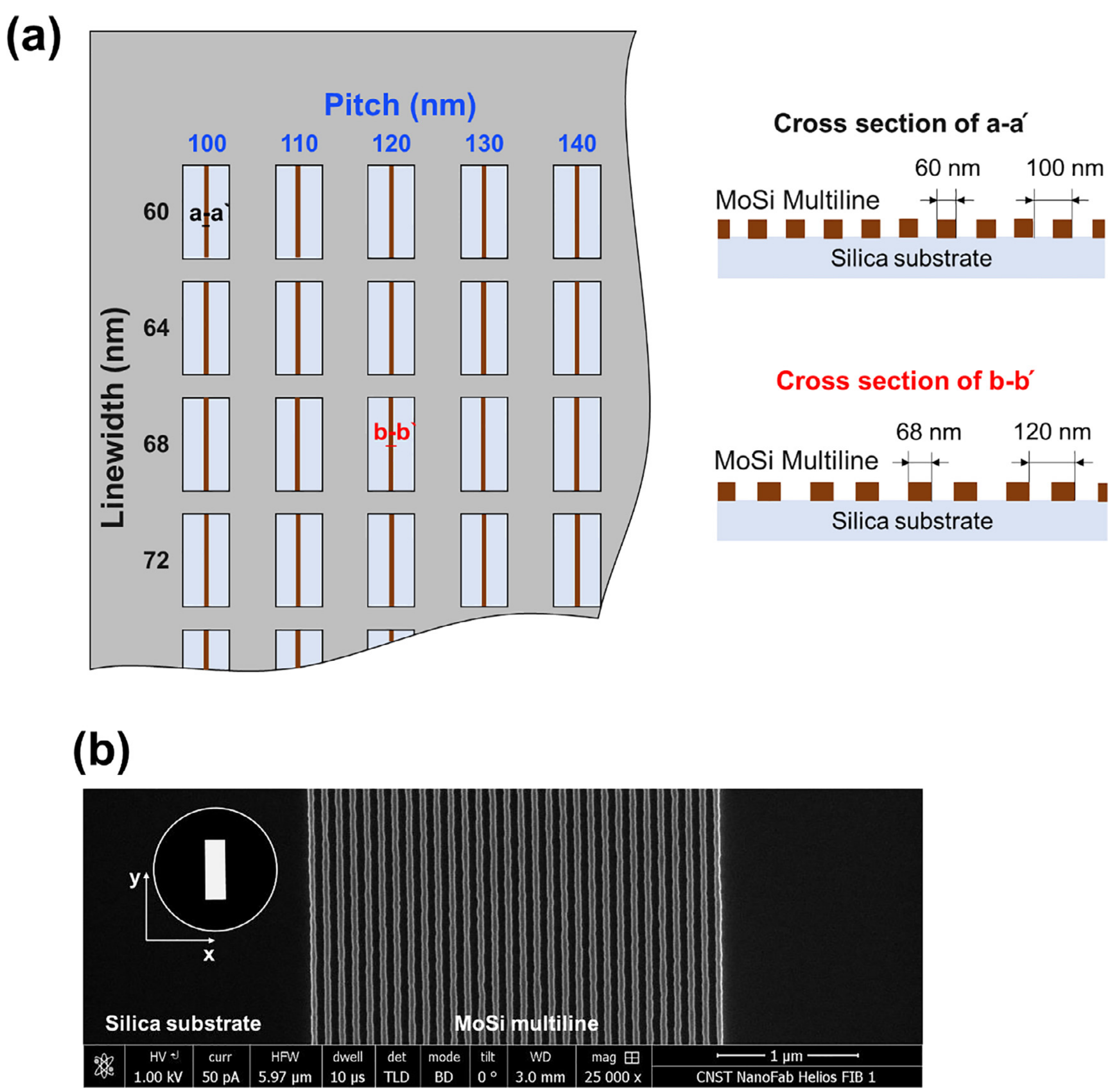

Fig. 3. Finite multiline targets on MoSi photomask. (a) Schematic of target arrangement for various linewidths and pitches. (b) SEM image of a target of 30 lines. The illumination aperture is aligned with respect to the line direction.

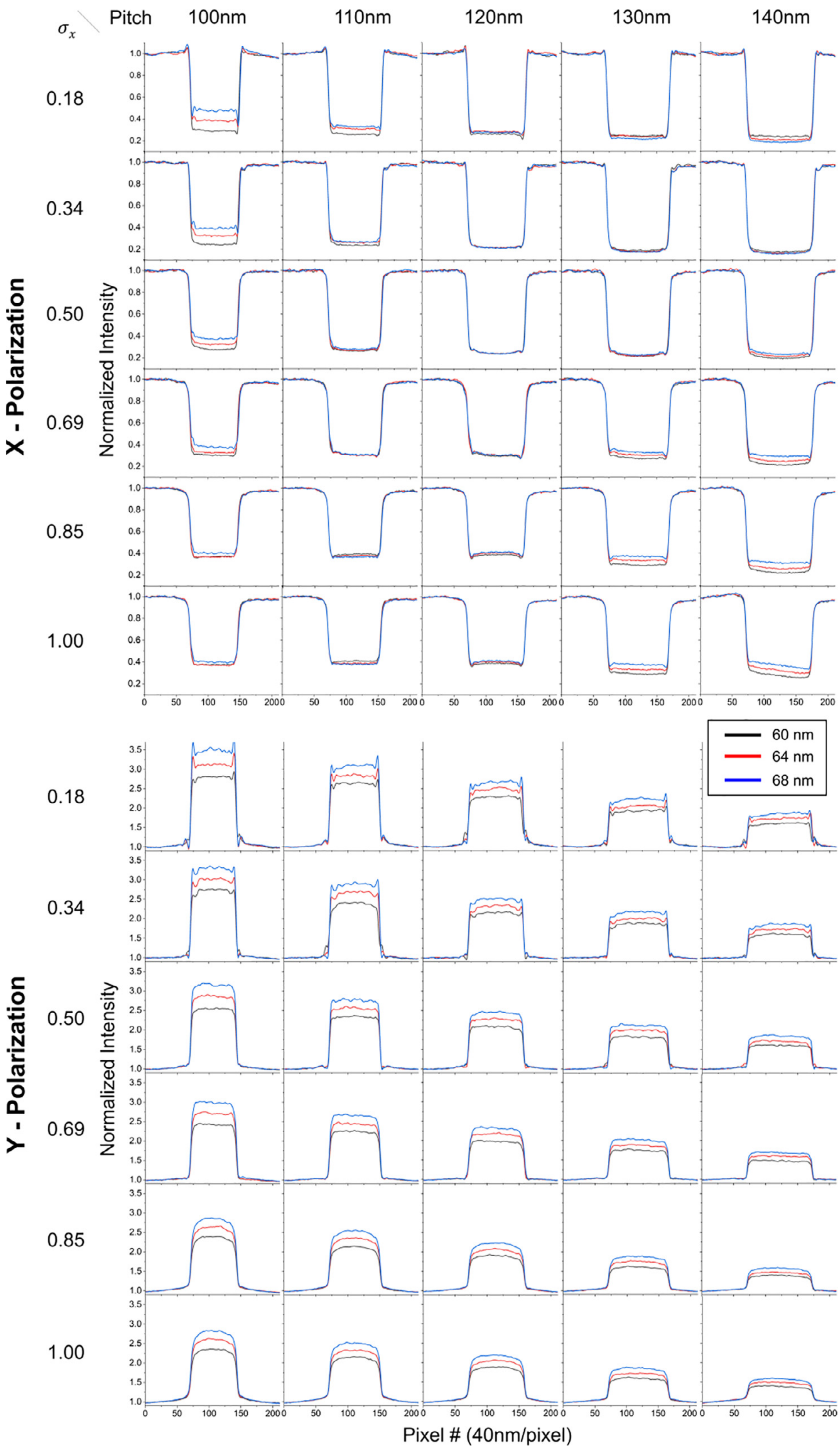

Fig. 4. Measured scatterfield intensity profiles for finite multiline targets. Columns and rows indicate the variations of pitch and partial coherence factor. The intensity differences $|I_{64}- I_{60}|$ and $|I_{68}- I_{64}|$ in each graph contribute to the measurement sensitivities.

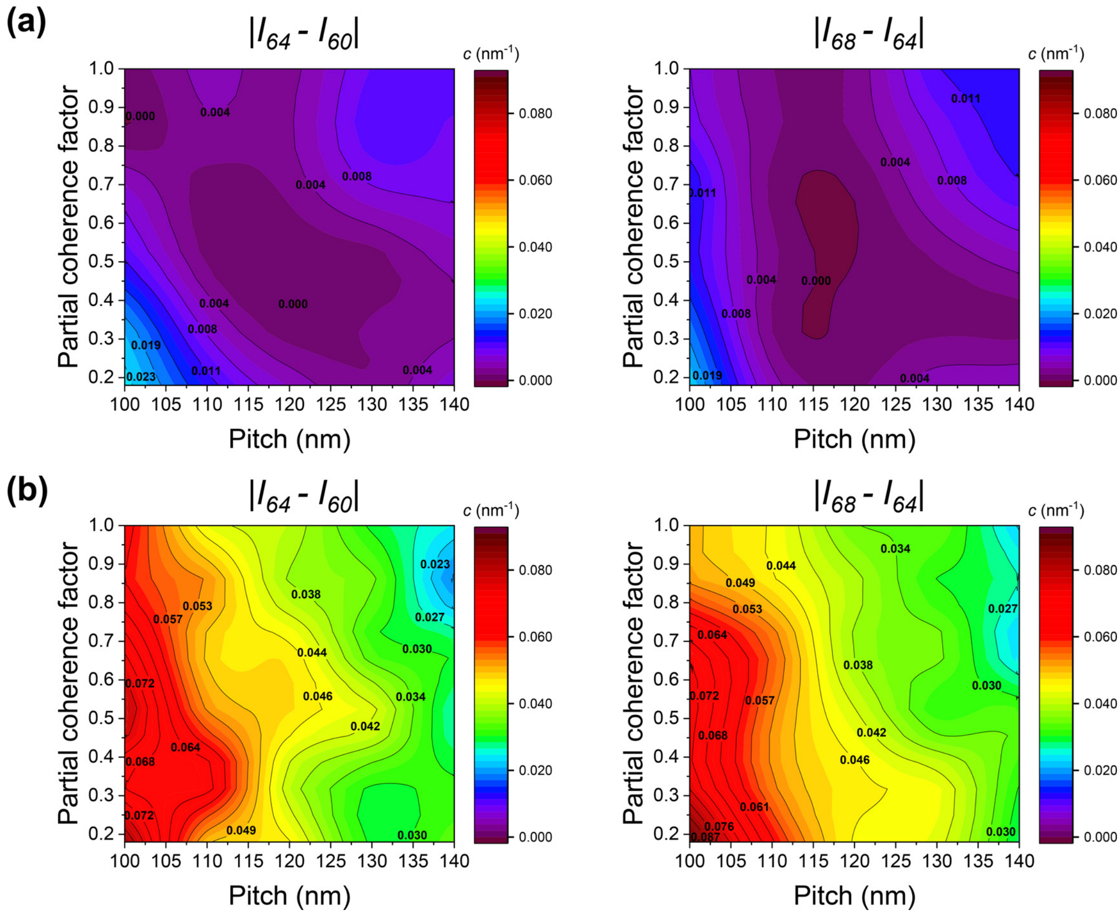

Fig. 5. Sensitivity coefficient distributions parameterized with partial coherence factor for (a) X- and (b) Y-polarizations. Two contour maps for each polarization are based on the measured intensity differences $|I_{64}- I_{60}|$ and $|I_{68}- I_{64}|$ for the linewidth pairs of 64 nm, 60 nm and 68 nm, 64 nm, respectively.

intensity profiles overlapped with the linewidths of 60, 64, and 68 nm, showing the scattered intensity differences which lead to a qualitative sensitivity evaluation. Larger intensity difference between the substrate and patterned area represents higher sensitivity in general. Each row arranges the graphs for the linewidth range of 100–140 nm with 10 nm increment, corresponding to 15 duty ratios of 0.429–0.680, which are defined by the ratio of linewidth to pitch, while each column contains the graphs for 6 partial coherence factors as shown in Fig. 2(b). As the linewidth changes at a fixed pitch, the intensity variation of the valley or hill is caused by line geometry-induced scatterfield distribution at a fixed angle cone of illumination. The intensities for both linewidth and pitch variations are influenced by both the line geometry and the angle of illumination.

For the quantitative evaluation of the measurement sensitivity, the sensitivity coefficient defined by Eq. (1) is calculated from two intensity profiles with linewidths of 60 nm and 64 nm ($|I_{64}- I_{60}|$) or 64 nm and 68 nm ($|I_{68}- I_{64}|$) as measurands. Thus, the sensitivity coefficient contour maps for the variations of partial coherence factor and duty ratio are obtained as shown in Fig. 5. A higher sensitivity coefficient value indicates a better measurement resolving power. Overall sensitivities with y polarization in Fig. 5(b) are higher than with x polarization in Fig. 5(a). Global maximum sensitivities for x polarization appear at lower pitches from 100 nm to 110 nm and lower partial coherence factors of around $\sigma_x = 0.18$, and local maximum sensitivities are found at the higher pitches around 135 nm to 150 nm and higher partial coherence factors of $\sigma_y = 0.9$–1.0. In contrast, the maps for y polarization show an obvious tendency that the sensitivity decreases as the pitch increases regardless of the partial coherence factor, which means that the scattered intensity does not depend on the illumination angle when the line and polarization directions coincide. The sensitivity maps provide a guidance for determining the optimum condition for illumination and target geometry for achieving high resolving power in measurement using the scatterfield imaging microscopy.

5. Conclusion

Measurement sensitivities of DUV scatterfield imaging microscopy for CD with various duty ratio were analyzed using a scatterfield imaging microscope platform using 193 nm Excimer laser source designed for highly resolved illumination. By tuning partial coherence factor for the multiline target of various duty ratios, we verified that the combination of partial coherence factor and duty ratio impacts the measurement sensitivity of CDs and the identification of optimum measurement conditions. Quantitative evaluation with sensitivity coefficient maps revealed that for x-polarization (perpendicular to the lines), better sensitivity is obtained at higher partial coherence (lower σ_x) for lower duty ratio and low partial coherence for higher duty ratio, whereas for y-polarization (parallel to the lines), the sensitivity becomes better as duty ratio decreases, being weakly affected by the partial coherence. These data show a sub-nanometer sensitivity to changes in linewidth with various line/space ratios, which will contribute to the advancement of controllability towards model-based nanoscale dimensional measurements using optimized illumination conditions.

Disclaimer

Certain commercial equipment, instruments, or materials are identified in this paper in order to specify the experimental procedure adequately. Such identification is not intended to imply recommendation or endorsement by the National Institute of Standards and Technology, nor is it intended to imply that the materials or equipment identified are necessarily the best available for the purpose.

Declaration of Competing Interest

The authors declare that they have no known competing financial interests or personal relationships that could have appeared to influence the work reported in this paper.

CRediT authorship contribution statement

Eikhyun Cho: Formal analysis, Investigation, Data curation, Writing – original draft, Visualization. **Taekyung Kim:** Formal analysis, Investigation, Data curation, Writing – original draft, Visualization. **Yoon Sung Bae:** Methodology, Software, Investigation, Data curation. **Sang-Soo Choi:** Resources, Data curation. **Bryan M. Barnes:** Software, Writing – review & editing. **Richard M. Silver:** Writing – review & editing, Funding acquisition, Project administration. **Martin Y. Sohn:** Conceptualization, Methodology, Validation, Formal analysis, Investigation, Writing – review & editing, Supervision, Project administration.

References

[1] Liddle JA, Gallatin GM. Lithography, metrology and nanomanufacturing. Nanoscale 2011;3:2679–88. doi:10.1039/c1nr10046g.

[2] Orji NG, Badaroglu M, Barnes BM, Beitia C, Bunday BD, Celano U, et al. Metrology for the next generation of semiconductor devices. Nat Electron 2018;1:532–47. doi:10.1038/s41928-018-0150-9.

[3] Asano M, Yoshikawa R, Hirano T, Abe H, Matsuki K, Tsuda H, et al. Metrology and inspection required for next generation lithography. Jpn J Appl Phys 2017;56:06GA01. doi:10.7567/JJAP.56.06GA01.

[4] Whitworth GL, Francone A, Sotomayor-Torres CM, Kehagias N. Real-time optical dimensional metrology via diffractometry for nanofabrication. Sci Rep 2020;10:5371. doi:10.1038/s41598-020-61975-3.

[5] Silver RM, Barnes BM, Attota R, Jun J, Stocker M, Marx E, et al. Scatterfield microscopy for extending the limits of image-based optical metrology. Appl Opt 2007;46:4248–57. doi:10.1364/AO.46.004248.

[6] Patrick HJ. Optical critical dimension measurement of silicon grating targets using back focal plane scatterfield microscopy. J Micro Nanolithogr MEMS MOEMS 2008;7(1):013012. doi:10.1117/1.2885275.

[7] Barnes BM, Attota R, Quintanilha R, Sohn YJ, Silver RM. Characterizing a scatterfield optical platform for semiconductor metrology. Meas Sci Technol 2011;22:024003. doi:10.1088/0957-0233/22/2/024003.

[8] Qin J, Silver RM, Barnes BM, Zhou H, Goasmat F. Fourier domain optical tool normalization for quantitative parametric image reconstruction. Appl Opt 2013;52:6512–22. doi:10.1364/AO.52.006512.

[9] Qin J, Silver RM, Barnes BM, Zhou H, Dixson RG, Henn MA. Deep subwavelength nanometric image reconstruction using fourier domain optical normalization. Light Sci Appl 2016;5:e16038. doi:10.1038/lsa.2016.38.

[10] Sun W, Ohta H, Ninomiya T, Goto Y. High-voltage CD-SEM-based application to monitor 3D profile of high-aspect-ratio features. J Micro Nanolithogr MEMS MOEMS 2020;19(2):024002. doi:10.1117/1.JMM.19.2.024002.

[11] Hussain D, Ahmad K, Song J, Xie H. Advances in the atomic force microscopy for critical dimension metrology. Meas Sci Technol 2017;28:012001. doi:10.1088/0957-0233/28/1/012001.

[12] Files-Sesler LA. Scanning tunneling microscopy: critical dimension and surface roughness analysis. J Vac Sci Technol B 1991;9:659–62. doi:10.1116/1.585481.

[13] Bazylewski P, Ezugwu S, Fanchini G. A review of three-dimensional scanning near-field optical microscopy (3D-SNOM) and its applications in nanoscale light management. Appl Sci 2017;7:973. doi:10.3390/app7100973.

[14] In Bodermann B, Buhr E, Li Z, Bosse H, Osten W, Reingand N. Quantitative optical microscopy at the nanoscale: new developments and comparisons. In: Optical imaging and metrology. Weinheim, Germany: Wiley-VCH Verlag GmbH & Co. KGaA; 2012. p. 255–82. doi:10.1002/9783527648443.ch12.

[15] Colonna de Lega X, Osten W, Reingand N. Model-based optical metrology. In: Optical imaging and metrology. Weinheim, Germany: Wiley-VCH Verlag GmbH & Co. KGaA; 2012. p. 283–304. doi:10.1002/9783527648443.ch13.

[16] Nguyen TH, Edwards C, Goddard LL, Popescu G. Quantitative phase imaging with partially coherent illumination. Opt Lett 2014;39(19):5511–13. doi:10.1364/OL.39.005511.

[17] Yu W, Wang S, Veetil S, Gao S, Liu C, Zhu J. High-quality image reconstruction method for ptychography with partially coherent illumination. Phys Rev B 2016;93:241105. doi:10.1103/PhysRevB.93.241105.

[18] Bae YS, Sohn MY, Lee DR, Choi SS. Effect of partial coherence on dimensional measurement sensitivity for DUV scatterfield imaging microscopy. Opt Express 2019;27(21):29938–48. doi:10.1364/OE.27.029938.

[19] Vagos P, Hu J, Liu Z, Rabello S. Uncertainty and sensitivity analysis and its applications in OCD measurements. Proc SPIE 2009;7272:72721N. doi:10.1117/1.602580.

[20] Ziger D, Leroux P. Understanding optical end of line metrology. Opt Eng 2000;39(7):1951–7. doi:10.1117/1.602580.

[21] Marciante JR, Farmiga NO, Hirsh JI, Evans MS, Ta HT. Optical measurement of depth and duty cycle for binary diffraction gratings with subwavelength features. Appl Opt 2003;42(16):3234–40. doi:10.1364/AO.42.003234.

[22] Verrina V, Edward S, Zhang H, Witte S, Planken PCM. Photoacoustic detection of low duty cycle gratings through optically opaque layers. Appl Phys Lett 2020;117:051104. doi:10.1063/5.0016078.

[23] Ausschnitt K, Truffert V, D'Have K, Leray P. Pattern shift response metrology. Proc SPIE 2018;1081:108100T. doi:10.1117/12.2502353.

[24] Ruffato G, Romanato F. Design of continuously variant metasurfaces for conformal transformation optics. Opt Express 2020;28(23):34201–17. doi:10.1364/OE.400627.

[25] Koehler A. New method of illumination for photomicrographical purposes. J R Microsc Soc 1894;14:261–2. doi:10.1111/j.1365-2818.1894.tb00027.x.

[26] Benner G, Probst W. Köhler illumination in the TEM: fundamentals and advantages. J Microsc 1994;174:133–42. doi:10.1111/j.1365-2818.1994.tb03461.x.

[27] Hsu W-T, Ku Y-S, Shyu D-M. A novel method for overlay measurement by scatterometry. Proc SPIE 2009;7432:74320F. doi:10.1117/12.825091.

[28] Hopins HH. The concept of partial coherence in optics. Proc R Soc Lond A 1951;208:263–77. doi:10.1098/rspa.1951.0158.

[29] Hopkins HH. On the diffraction theory of optical images. Proc R Soc Lond A 1953;217:408–32. doi:10.1098/rspa.1953.0071.

[30] Gbur G, Visser TD. The structure of partially coherent fields. In: Progress in optics, 55. Elsevier; 2010. p. 285–341. doi:10.1016/B978-0-444-53705-8.00005-9.

[31] Smith BW. The Saga of Sigma: influences of illumination throughout optical generations. Proc SPIE 2014;9052:905204. doi:10.1117/12.2048827.

[32] Singh M, Lajunen H, Tervo J, Turunen J. Imaging with partially coherent light: elementary-field approach. Opt Express 2015;23(22):28132–40. doi:10.1364/OE.23.028132.

[33] Kintner EC, Sillitto RM. Edge-ringing in partially coherent imaging. Opt Acta Int J Opt 1977;24:591–605. doi:10.1080/713819597.

[34] Taylor BN, Kuyatt CE. Guidelines for evaluation and expressing the uncertainty of NIST measurement results. NIST Technical Note 1297 National Institute of Standards and Technology; 1994 https://emtoolbox.nist.gov/Publications/NISTTechnicalNote1297s.pdf.

[35] Farrance I, Frenkel R. Uncertainty of measurement: a review of the rules for calculating uncertainty components through functional relationships. Clin Biochem Rev 2012;33(2):49–75. https://www.ncbi.nlm.nih.gov/pmc/articles/PMC3387884/.

[36] Takeda S, Kitada T. Simple method based on sensitivity coefficient for stochastic uncertainty analysis in probabilistic risk assessment. Reliab Eng Syst Saf 2021;209:107471. doi:10.1016/j.ress.2021.107471.

[37] Horibe M, Kon S, Hirano I. Measurement capability of scanning microwave microscopy: measurement sensitivity versus accuracy. IEEE Trans Instrum Meas 2019;68:1774–80. doi:10.1109/TIM.2018.2882937.

[38] Sohn MY, Barnes BM, Silver RM. Design of angle-resolved illumination optics using nonimaging bi-telecentricity for 193 nm scatterfield microscopy. Optik 2018;156:635–45 (Stuttg). doi:10.1016/j.ijleo.2017.11.206.

[39] Liba O, Lew MD, SoRelle ED, Dutta R, Sen D, Moshfeghi DM, et al. Speckle-modulating optical coherence tomography in living mice and humans. Nat Commun 2017;8:15845. doi:10.1038/ncomms15845.

[40] Stangner T, Zhang H, Dahlberg T, Wiklund K, Andersson M. Step-by-step guide to reduce spatial coherence of laser light using a rotating ground glass diffuser. Appl Opt 2017;56(19):5427–35. doi:10.1364/AO.56.005427.